Ultrashort elastic and plastic shockwaves in aluminum

Nail Inogamov, Viktor Khokhlov, Yurii Petrov, Sergey Anisimov, Vasily V. Zhakhovsky et al.

Citation: AIP Conf. Proc. **1426**, 909 (2012); doi: 10.1063/1.3686425
View online: http://dx.doi.org/10.1063/1.3686425
View Table of Contents: http://proceedings.aip.org/dbt/dbt.jsp?KEY=APCPCS&Volume=1426&Issue=1
Published by the American Institute of Physics.

ULTRASHORT ELASTIC AND PLASTIC SHOCK WAVES IN ALUMINUM

Nail A. Inogamov[*], Viktor A. Khokhlov[*], Yurii V. Petrov[*], Sergey I. Anisimov[*], Vasily V. Zhakhovsky[†], Brian J. Demaske[†], Ivan I. Oleynik[†], Carter T. White[**], Sergey I. Ashitkov[‡], Konstantin V. Khishchenko[‡], Mikhail B. Agranat[‡] and Vladimir E. Fortov[‡]

[*]*Landau Institute for Theoretical Physics, RAS, Chernogolovka 142432, Russian Federation*
[†]*Department of Physics, University of South Florida, Tampa, FL, 33620, USA*
[**]*Naval Research Laboratory, Washington, DC 20375, USA*
[‡]*Joint Institute for High Temperatures, RAS, Moscow 125412, Russian Federation*

Abstract. Ultrashort shock waves in aluminum films generated by femtosecond laser pulses were studied using two-temperature hydrodynamics and molecular dynamics methods. We observed double wave breaking characterized by an independent formation of leading elastic and trailing plastic shock waves. Both the amplitude and speed of the plastic shock decrease quickly in time due to hydrodynamic attenuation, while the elastic shock front slowly decays during propagation. When the pressure in the plastic front becomes equal to the normal component of pressure tensor in the elastic zone, the plastic wave disappears. Therefore, the distance between elastic and plastic fronts first decreases, then increases, with time. The elastic shock uniaxially compresses the crystal to pressures higher than the Hugoniot elastic limit (HEL). For a short time, the crystal within the elastic zone remains in a metastable state, that lies on an extension of the elastic branch of the Hugoniot beyond the HEL. Our theoretical results explain the seemingly puzzling experimental findings, where high-pressure elastic shock waves were observed with normal pressures up to 10–20 GPa.
Keywords: Elastic-plastic shock splitting, femtosecond laser shock generation
PACS: 62.50.Ef, 79.20.Eb, 02.70.Ns

INTRODUCTION

Strong elastic shock waves (ESWs) recently observed in several micron thick aluminum films exhibited normal pressures p_{xx} up to 12 GPa [1–3], much higher than the ~ 0.3 GPa pressure exhibited by elastic shock wave precursors in many millimeter thick Al films [4]. Main obstacles impeding the earlier discovery of strong ESWs were the time $(200-300$ ps$)$ and space $(2-3\ \mu$m$)$ resolution of VISAR (Velocity Interferometer System for Any Reflector) systems commonly used for diagnostics in shock wave (SW) experiments. The minimum temporal and spatial splittings between elastic and plastic shock waves that could be experimentally resolved were too large to capture a strong ESW. Pump-probe methods with multiple-repetition microscope interferometry (MRMI) [1, 5] and single-shot microscope interferometry (SSMI) [2, 3] have greatly improved the experimental resolution [0.1 ps for MRMI (See Refs. [1, 5], and references cited therein.) and a few ps for SSMI]. Such ultrafast chirped pulse methods have made possible the observation of *strong* ESWs. Below is a list of the experiments:

- Pure ESW in Al, MRMI [1]
- Pure elastic SW in Ni, MRMI [6]
- Elastic-plastic splitting in Al (2, 5, and 8 μm thick films, long drive, SSMI) [3]
- Elastic-plastic splitting in Al, MRMI [7]

Shock Compression of Condensed Matter - 2011
AIP Conf. Proc. 1426, 909-912 (2012); doi: 10.1063/1.3686425

- Elastic-plastic splitting in Al film of 9 μm thick (Only SW arrival at the rear side of the film has been measured.) [8]

Strong ESWs were observed in piston [9–11] and moving window [11] molecular dynamics (MD) simulations. Herein, we link the MD results to femtosecond (fs) laser experiments using a description of the laser piston obtained from a two-temperature (2T) physical model of the fs laser-metal interaction, where initially the electron T_e and ion T_i temperatures are not equal following the pulse and equilibrate as the shock wave develops. The existence of strong ESWs is supported by the agreement obtained between theory and fs experiments.

MODELING METHODS AND RESULTS

Femtosecond chirped laser SW generators are promising tools for studies of SW propagation. To simulate their effect it is necessary to apply a 2T physical model of the metal under fs laser irradiation. In our work, a combined 2T-HD/MD approach is used [12]. The 2T physics includes the 2T equation of state of Al and a description of the electron-ion energy exchange and 2T heat conduction taken from Ref. [13]. The electron-ion energy coupling coefficient α is taken from Ref. [14], similar to the one used in Ref. [15]. Also, see Ref. [16].

The calculations presented in Figs. 1–2 are for a pump pulse duration $\tau_L = 0.1$ ps and absorbed energy of 2.6 J/cm^2 [7, 8]. Computed trajectories of the melting front, the ESW, and plastic shock wave (PSW) along the $x = [110]$ crystallographic axis normal to the surface of the film are shown in these figures. Because the diameter of the irradiated spot is much larger than the film thickness, the motion is 1D.

The laser energy absorption stage occupies a very small time-space domain $\tau_L \times \delta_{skin}$, where $\delta_{skin} \approx$ 15 nm is the penetration depth in Al and $\tau_L = 0.1$ ps for the Ti:Sapphire and Cr:Forsterite lasers used. This domain is small even on the scale of Fig. 1, which is reduced in comparison to Fig. 2. Nevertheless, such a high energy concentration has large effects over a much wider domain with the production of powerful SWs and significant molten and plastically modified layers. See Fig. 2.

Calculated maximal electron and ion temperatures (T_e[eV], T_i[eV]) are (15.7, 1.1), (9.9, 2.2), (5.45, 3.1), and (2.24, 2.1) for times 0.3, 1, 3, and 10 ps after the maximum of the Gaussian pump pulse. Hence, electron-ion temperature relaxation takes $t_{eq} \approx 5$ ps. During relaxation, the 2T flow, dominated by heat diffusion, transfers to 1T hydrodynamic flow with little influence from heat diffusion (1T $\equiv$ one-temperature: $T_e = T_i$).

Acceleration of the material to an acoustic velocity $u \sim p/c_s\rho$, where ρ is the density and c_s the sound speed, takes place while the pressurized layer decays into a Riemann compression wave. During t_{eq}, the flow regime changes from supersonic heat diffusion to nonlinear acoustic motion [17]. By $\sim t_{eq}$ the heat wave decelerates from supersonic to subsonic speed and a Riemann wave is generated. See Fig. 1. This nonlinear, high-amplitude Riemann wave, with pressure greater than bulk modulus for Al, evolves during propagation through focusing of its characteristics [17]. As the characteristics begin to intersect, the Riemann wave breaks and the main PSW forms.

The melting front is also supersonic at the 2T stage. Eventually, it becomes subsonic and emits acoustic perturbations, because the compressibility of matter changes during the melting [17]. Simulations show that these perturbations evolve into the ESW. Therefore, the experimental results shown by diamonds and circles in Fig. 1 indirectly indicate that supersonic melting takes place.

With time the PSW attenuates, and in the course of transformation to a transonic regime emits the acoustic wave (AW) shown in Fig. 2. Interestingly, the AW does not form tangential to the curved trajectory of the PSW front passing from the supersonic to subsonic regime of propagation. At the triple intersection PSW – EP – AW, the PSW still exhibits a pressure jump, but its propagation velocity (4.3 km/s) is about half that of the acoustic wave AW (8.2 km/s) in elastic Al. Finally, the pressure in the PSW drops to the normal pressure p_{xx} in the ESW, and the PSW decays to a subsonic front EP separating elastic and plastic regions of Al that moves slowly in the unloading tail of the ESW and soon stops. EP is not a shock wave but is a transition layer several tens of nanometers thick between elastic and plastic regions, where new dislocations are slowly generated by the existing dislocations until the local stress drops below the yield stress in this layer. Important other observations are:

- Almost linear propagation of the ESW with a

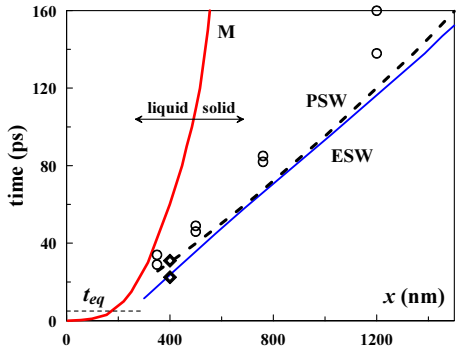

FIGURE 1. Transition from 2T stage (scales are $t_{eq} \sim$ 5 ps and $\sim$ 200 nm) to 1T regime, and formation of the ESW and the PSW. Distance between the ESW and the PSW passes through a minimum at $t_{min} = 65$ ps. Curve M is a melting front from the 2T hydrodynamics simulation. Two diamonds give positions of ESW and PSW in experiment [7]. Pairs of circles correspond to ESW and PSW in our experiments (see also [21]) with $F_{abs} \approx 2$ J/cm^2, slightly smaller than in our simulations and Ref. [7].

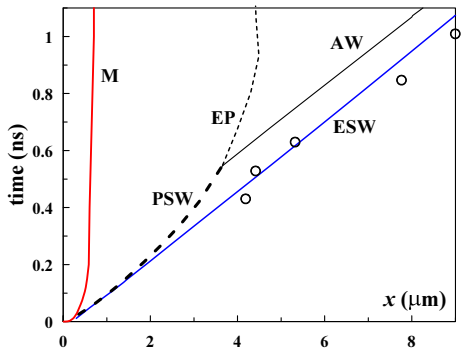

FIGURE 2. Trajectories of ESW, PSW, and melting front M at the micron scale. Circles are experimental points [8]. EP is a subsonic transition layer separating elastic and plastic regions of Al propagating in the unloading tail of the ESW, where new dislocations are slowly generated by the existing dislocations. The film is plastically deformed to a depth of $d_{pl} \approx 4.4$ μm, when EP has stopped.

deceleration time of $D/(dD/dt) \approx 15$ ns, where $D(t)$ is velocity of the ESW, $D(t = 0.3 - 1\text{ ns}) = 8.2 - 8$ km/s. The normal pressure behind the ESW decreases from 16 to 12 GPa during first 0.6 ns. Thus, the ESW propagates ≈ 20 microns during ≈ 2.4 ns before the pressure falls from 16 to 1 GPa.

- The thickness of the plastically modified surface layer d_{pl} depends on the absorbed fluence F_{abs}, where $d_{pl} \approx 4.4$ μm. For the case treated in Figs. 1 and 2, the maximum thickness of the molten zone is 0.7 μm. See Fig. 2.

The agreement between experiments and simulations indicates that strong elastic waves, although not mentioned at the time, were produced in the experiments [6–8]. The existence of such strong ESWs now is widely appreciated [1, 3, 18, 19] by both theorists and experimentalists. See also, Refs. [20–23].

STRONG ELASTIC SHOCK WAVES: HOW PERSISTENT?

The papers [1–3, 18, 19] establish the existence of anomalously strong ESWs in crystalline solids. However, are these ESWs transients caused by the initial impulse subsequently overrun by the PSW or can they persist to longer times, even if constantly overdriven to pressures significantly higher than the HEL? In the past, it was often thought that the pressure within the elastic zone would necessarily decay to the HEL. Whereupon, the elastic front would be either overrun by the PSW, if overdriven, leading to a one-wave one-zone (1W1Z) pure plastic SW structure, or separate from the PSW at constant speed, if underdriven, leading to a split two-wave, two-zone (2W2Z) elastic-plastic SW structure. In the latter case, the ESW persists but the pressure in the elastic zone does not exceed the HEL. However, in addition to these standard 1W1Z and 2W2Z structures, it has recently been predicted that there will also exist an intermediate one-wave two-zone (1W2Z) elastic-plastic SW structure, where the elastic and plastic shock fronts both propagate at the same speed, the elastic zone supports a pressure significantly higher than the HEL, and the constant average thickness of the elastic zone can be appreciable [11]. In terms of supporting piston pressure, the 1W2Z structure lies between the well-known 2W2Z and 1W1Z structures.

Full 2T-HD/MD [12] simulations of our experiments and those of Ref. [7] lead to results in good agreement, as shown in Fig. 1. The duration of the parallel part of the trajectories of the co-moving ESW and PSW in Fig. 1 is $t_{stat} \approx 60$ ps. During this

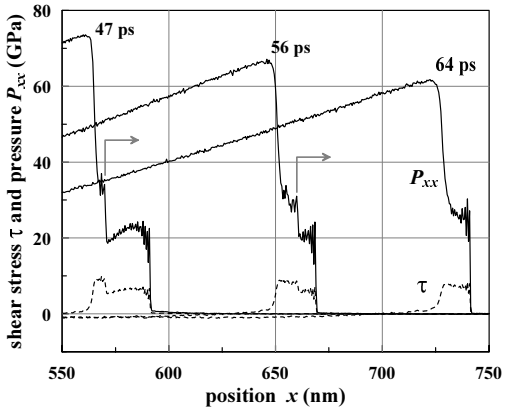

FIGURE 3. Snapshots of a 1W2Z structure from the simulations including an elastic pulse emitted by the PSW. Propagation of this pulse is indicated by the arrows. The position of the leading elastic front is shown in Fig. 1. The thickness of the pressure rise range in the PSW is $3-6$ nm. The profile $p_{xx}(x)$ at $t = 64$ ps corresponds to the minimal length of the elastic zone. See Fig. 1.

time the separation d_{el} between SWs increases by a factor of two from its minimal value $d_{el}(t_{min} = 65\,\text{ps})|_{min} = 12$ nm. The time t_{stat} is much larger than the minimum of the residence time $t_L \approx 2$ ps, required for a Lagrangian particle to pass through the elastic zone. Compare d_{el} and the gradient of p in the plastic zone in Fig. 3. Consequently, this could be close to a 1W2Z structure with strong coupling [11] between the ESW and the PSW.

The coupling between elastic and plastic shock fronts arises from elastic pulses emitted from the PSW front. When a Lagrangian particle in the elastic state arrives at the PSW, it slows and compresses along the Rayleigh line toward the density in the PSW. Because the elastic-plastic transformation takes a finite time, the particle cannot instantly jump to a state on the plastic branch of the Hugoniot. Thus, transient elastic states between the elastic and plastic branches of the Hugoniot are produced. The particle in the transient elastic state has a higher pressure than in the elastic zone ahead. As a result, this particle emits an elastic pulse before transformation to a plastic state. Such an elastic pulse is highlighted by the arrows in Fig. 3.

Finally, a 2T-HD/MD [12] simulation of the experiment [3] is beyond the scope of the current work, as it must include the energy transfer from hot metal to glass at the metal-glass interface during the laser pulse. Nevertheless, an estimate of the residence time from Fig. 6 of Ref. [3], $t_L \sim d_{el}/c_s \sim 70$ ps, leads to a value ~ 10 times less than the time variation of plastic pressure $p/(dp/dt) \approx 1$ ns. Therefore, results of Ref. [3] could lie largely in the 1W2Z regime.

This work was supported by ONR, NRL, and NSF. The Russian team was supported by the RFBR grant 10-02-00434-a.

REFERENCES

1. Ashitkov, S. I., Agranat, M. B., Kanel', G. I., *et al.*, *JETP Lett.,* **92,** 516-20 (2010).
2. Armstrong, M. R., Crowhurst, J. C., Bastea, S., and Zaug, J. M., *J. Appl. Phys.*, **108**, 023511 (2010).
3. Whitley, V. H., McGrane, S. D., Eakins, D. E., Bolme, C. A., *et al.*, *J. Appl. Phys.*, **109**, 013505 (2011).
4. Kanel, G. I., Razorenov, S. V., and Fortov, V. E., *Shock-Wave Phenomena and the Properties of Condensed Matter*, Springer, 2004
5. Temnov, V. V., Sokolowski-Tinten, K., *et al.*, *J. Opt. Soc. Am. B,* **23**, 1954-64 (2006).
6. Gahagan, K. T., Moore, D. S., Funk, D. J., *et al.*, *Phys. Rev. Lett.,* **85,** 3205-8 (2000).
7. Evans, R., et al, *Phys. Rev. Lett.,* **77,** 3359-62 (1996).
8. Huang, Li, et al, *J. Phys. D,* **42,** 045502 (2009).
9. Kadau, K., Germann, T. C., Lomdahl, P. S., and Holian, B. L., *Phys. Rev. B,* **72,** 064120 (2005).
10. Bringa, E. M., Rosolankova, K., Rudd, R. E., *et al.*, *Nat. Mater.,* **5,** 805-9 (2006).
11. Zhakhovsky, V., Budzevich, M., Inogamov, N., Oleynik, I., and White, C., (in press, *Phys. Rev. Lett.*).
12. In our approach the 2T hydrodynamics code (2T-HD) is combined with the MD code [18, 19].
13. Inogamov, N., Petrov, Yu., *JETP,* **110,** 446-68 (2010).
14. Petrov, Yu. V., *Las. Part. Beams,* **23,** 283-289 (2005).
15. Lin, Z., et al, *Phys. Rev. B,* **77,** 075133 (2008).
16. Inogamov, N. A., Faenov, A. Ya., Zhakhovsky, V. V., *et al.*, *Contrib. Plasma Phys.,* **51,** 419-26 (2011).
17. Inogamov, N. A., Zhakhovsky, V. V., Ashitkov, S. I., *et al.*, *Contrib. Plasma Phys.,* **51,** 367-374 (2011).
18. Zhakhovskii, V. V. and Inogamov, N. A., *JETP Lett.,* **92,** 521-6 (2010).
19. Inogamov, N. A., Zhakhovskii, V. V., Khokhov, V. A., and Shepelev V. V., *JETP Lett.,* **93,** 226-32 (2011).
20. Crowhurst, J., Armstrong, M., Knight, K., *et al.*, AIP SCCM Conf. Proc. (2011), T3.3
21. Ashitkov, S., Agranat, M., Kanel, G., *et al.*, AIP SCCM Conf. Proc. (2011), Y1.5
22. Zhakhovsky, V. V., *et al.*, (in press, *Phys. Rev. Lett.*); see also in AIP SCCM Conf. Proc. (2011), J3.1
23. Demaske, B. J., *et al.*, AIP SCCM Conf. Proc. (2011), B3.1 and V3.2